Andean Geology
ISSN: 0718-7092
ISSN: 0718-7106
andeangeology@sernageomin.cl
Servicio Nacional de Geología y Minería
Chile

Geochemical characteristics of the infilling of ground wedges at Puerto Deseado (Santa Cruz, Argentina): palaeoenvironmental and chronological implications

Zanchetta, Giovanni; Ribolini, Adriano; Ferrari, Matteo; Bini, Monica; Isola, Ilaria; Lezzerini, Marco; Baroni, Carlo; Salvatore, Maria Cristina; Pappalardo, Marta; Fucks, Enrique; Boretto, Gabriella

Geochemical characteristics of the infilling of ground wedges at Puerto Deseado (Santa Cruz, Argentina): palaeoenvironmental and chronological implications

Andean Geology, vol. 45, no. 2, 2018

Servicio Nacional de Geología y Minería, Chile

Available in: https://www.redalyc.org/articulo.oa?id=173955659002

DOI: https://doi.org/10.5027/andgeoV45n2-3070

Artículos de Investigación

Geochemical characteristics of the infilling of ground wedges at Puerto Deseado (Santa Cruz, Argentina): palaeoenvironmental and chronological implications

Características geoquímicas de las cuñas de hielo en Puerto Deseado (Santa Cruz, Argentina): implicancias paleoambientales y cronológicas

DOI: https://doi.org/10.5027/andgeoV45n2-3070
Redalyc: https://www.redalyc.org/articulo.oa?id=173955659002

Giovanni Zanchetta
Istituto Nazionale Geofisica e Vulcanologia Roma, Italia
zanchetta@dst.unipi.it

Adriano Ribolini
University of Pisa, Italia
ribolini@dst.unipi.it

Matteo Ferrari
University of Pisa, Italia
jason88kill@yahoo.it

Monica Bini
Istituto Nazionale Geofisica e Vulcanologia Roma, Italia
bini@dst.unipi.it

Ilaria Isola
Istituto Nazionale di Geofisica e Vulcanologia, Italia
ilaria.isola@ingv.it

Marco Lezzerini
University of Pisa, Italia
lezzerini@dst.unipi.it

Carlo Baroni
University of Pisa, Italia
baroni@dst.unipi.it

Maria Cristina Salvatore
University of Pisa, Italia
mariacristina.salvatore@unipi.it

Marta Pappalardo
University of Pisa, Italia
pappalardo@dst.unipi.it

Enrique Fucks
Universidad Nacional de La Plata, Argentina
efucks@fcnym.unlp.edu.ar

Gabriella Boretto
CICTERRA, Argentina
gmboretto@yahoo.com.ar

Received: 22 May 2017
Accepted: 18 October 2017

Abstract:

Ground wedge structures of cryogenic origin are common in the Quaternary sediments along the coast of the Patagonia, and their formation is related to climatic cold events experienced by this area in the Late Quaternary. The infilling sediments of two wedges generations were analyzed in the area of Puerto Deseado. Bulk chemistry (major elements), X-ray diffraction (XRD), morphoscopic observations with Scanning Electronic Microscope (SEM) and chemical analyses of volcanic glass shards were undertaken to provide indications about infilling sediment provenience, along with chronological constraint for wedge formation. Bulk chemistry and XRD patterns indicate a significant SiO_2 - enriched composition of the sediment infilling compared to the most of the loess deposits of the North Argentina and the present day dust originated in Patagonia. This was interpreted as due to the nature of the bedrock present over the Deseado Massif. SEM morphoscopic characteristics of glass shards evidence typical aeolian reworking features, with impact structures and indented edges of the volcanic fragments. Chemical analyses of the glass shards indicate that they were probably generated by the H_0 eruption (17,300-17,400 cal yr BP) of the Hudson volcano. Volcanological data indicate that H_0 eruption dispersed toward NE, but volcanic glasses were available for reworking due to a WNW component in the western wind direction. Over the Deseado Massif structural high the glass shards mixed with sediments enriched in SiO_2 , and were eventually deflated further to SE reaching the present coastal area and infilling the frost cracks. The age of the glass shards (17,300-17,400 cal yr BP) and that of the sandy layer affected by cryogenic structures (14,670±750 yr BP) well constrain to the Late Glacial both wedge generations.

Keywords: Hudson volcano, Geochemistry, XRD, SEM/EDS, Wedge structure, Quaternary sediments, Patagonia.

Resumen:

Las cuñas de hielo son estructuras comunes en sedimentos cuaternarios a lo largo de la costa patagónica, y su formación está relacionada con eventos climáticos fríos experimentados en esta área en el Cuaternario Tardío. Se analizaron sedimentos que rellenan dos generaciones de cuñas de hielo en la zona de Puerto Deseado. Análisis químicos de elementos mayores, difractometría de rayos X (DRX), observaciones con microscopio electrónico de barrido (SEM) y análisis químico de fragmentos de vidrio volcánico contenidos en el sedimento que rellena las cuñas proporcionaron información sobre la precedencia del relleno, además de inferir antecedentes cronológicos sobre su formación. La composición química del sedimento y la difracción de rayos X indican una composición enriquecida en SiO_2 en comparación con la mayoría de los depósitos de loess del norte de Argentina y el polvo actual originado en la Patagonia. Esto fue interpretado como producto de la influencia de las rocas que constituyen el macizo del Deseado. Las características morfológicas de los fragmentos de vidrio evidencian rasgos típicos de retrabajo eólico, con presencia de estructuras de impacto y bordes dentados. Los análisis químicos de los fragmentos de vidrio son compatibles con un origen en la erupción H_0 (17.300-17.400 cal yr BP) del volcán Hudson. Datos volcanológicos indican que la erupción H_0 originó una pluma de dispersión hacia el NE. El material volcánico dispersado por esta erupción quedó disponible para ser retrabajado por una componente WNW de los vientos del W dominantes en la zona. Sobre el macizo del Deseado, los fragmentos de vidrio se mezclaron con sedimentos ricos en SiO_2 y fueron adicionalmente, enriquecidos en este elemento hasta alcanzar el área de costa actual, rellenando las cuñas de hielo. La edad de los fragmentos de vidrio (17.300-17.400 cal yr BP) y de la capa arenosa afectada por las estructuras criogénicas (14.670±750 años BP) limitan al glacial tardío la formación de ambas generaciones de cuñas.

Palabras clave: Volcán Hudson, Geoquímica, XRD, SEM/EDS, Cuñas de hielo, Sedimentos cuaternarios, Patagonia.

1. Introduction

In cold environments, ground temperatures below the freezing point may generate a tensile stress causing thermal cracks in the frozen material (Lachenbruch, 1962). The frost cracks may be limited to the surface seasonally frozen layer or affect the perennial frozen sediments beneath (i.e., permafrost) (Williams and Smith, 1989; French, 2011). Irrespectively of their origin, frost cracks may be infilled by water eventually frozen or sediments (i.e., sand), originating a suite of wedge-shaped sedimentary structures that in the case of seasonal features are named "ground wedges" (Murton et al., 2000; French et al., 2009). The infilling of ground wedge is commonly locally derived, but long distance proveniences cannot be excluded a priori in the environments where rapid geomorphological processes are dominant (i.e., aeolian).

In summary, although ground wedges cannot be considered per se an indicator of permafrost, their existence and the definition of infillings characteristics (i.e., grain-size, quartz-grain texture, chemistry)

provide relevant elements supporting and complementing the reconstructions of past cold environments (Murton and Koulstrup, 2003; French, 2011).

In southernmost Atlantic South America Late Quaternary, ground wedge structures have been documented in Tierra del Fuego (Coronato et al., 2004; Pérez Alberti et al., 2008) and in Patagonia (e.g., Trombotto, 2002; Brockheim et al., 2009).

Recently, at Puerto Deseado (Santa Cruz Province, Argentina) (Fig. 1), Ribolini et al. (2014) described two different generations of ground wedges, chronologically constrained to the Late Glacial. Ribolini et al., (2014) also noted the presence of volcanic glass shards within the sedimentary infilling and advanced some hypothesis on the possible sources of these tephra. With the aim to better characterize the sedimentary infill and the origin of the volcanic material, we report the geochemistry of the infilling sediment and of that of the volcanic glass shard. These analyses can provide palaeoenvironmental information of regional relevance (i.e., provenience) and chronological constraints to wedge formation that is well-known difficult to be dated.

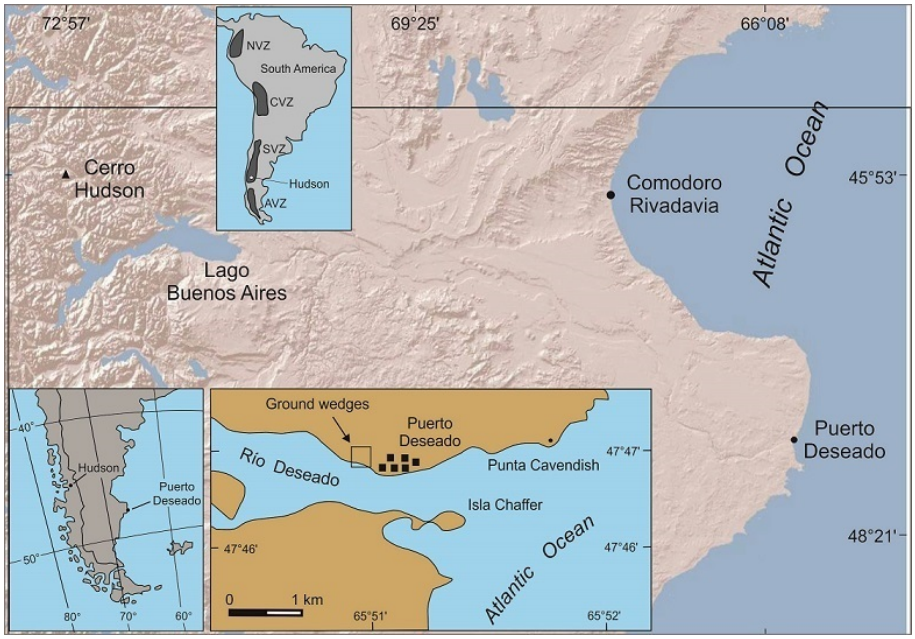

FIG. 1.

FIG. 1. Location maps. NVZ: North volcanic Zone; CVZ: Central volcanic zone; SVZ: South volcanic Zone; AVZ: Austral volcanic zone.

2. The previous works on Tierra del Fuego and Patagonian wedges

Following the pioneering work of Czaika (1955), frost wedging phenomena have been widely described in the Tierra del Fuego and Patagonia (e.g., Trombotto, 2002; Brockheim et al., 2009 and references therein). In the Southern Patagonia, sand wedges have been associated to some of the glacial phases that have been alternating since 1.5 Ma in the Southern hemisphere (Brockheim et al., 2009). According to the authors, these features formed inside glacial and fluvioglacial deposits coeval with the glacier advances that approached the Atlantic coast. The definition of the grain-size of sandy infillings allowed to extrapolate that during these cold phases the environment was dominated by wind action. Only morphostratigraphic correlations have been employed to date the formation of these sedimentary features, and frost wedges clearly attributed to the Last Glacial Maximum (LGM) and the Late Glacial (LG) cold events are not described.

Moving to the north, the various cryogenic features observed in the Patagonia region have been reviewed by Trombotto (2002), and in general LGM frost wedges along the Atlantic coastal areas resulted very limited and no attributions to LG cold events are clearly reported. The stratigraphic context of the features described

in the inland of Puerto Deseado suggests a LGM formation (Schellmann, 1998), but this hypothesis remains to be chronologically demonstrated. Further to the North, in the area of Puerto Madryn, according to Vogt and del Valle (1994) sedimentological, pedostratigraphical and geochemical data supported the existence of frost wedges whose infilling was supposed alimented by easterly winds deflating a marine platform exposed during sea level lowstand. However, the age of these wedges is controversial and it has been re-evaluated by Trombotto and Ahumada (1995) and considered much older than the initial attribution to the LGM (Corte and Beltramone, 1984).

2.1. The wedges in the Puerto Deseado area

The study area is located in the so-called Deseado massif (Ramos and Ghiglione, 2008), characterized by the extensive outcrops of middle-upper Jurassic volcanic and volcanoclastic rocks of the Chon-Aike Formation of the Bahía Laura Group (Guido et al., 2004; Sruoga et al., 2004). These rocks are mainly calc-alkaline peraluminous rhyolites, with some dacitic members (Pankhurst and Rapela, 1995; Pankhurst et al., 1998), displaying a prevalent massive aspect (welded ignimbrites). The principal minerals components are quartz, K-feldspar, plagioclase and biotite; accessories are magnetite, ilmenite, apatite and zircon with associated monazite (Sruoga et al., 2004).

According to Ribolini et al. (2014) the wedge structures formed within continental deposits (slope, fluvial and loess deposits) covering coarse (gravelly) coastal marine sediments correlated to MIS5e highstand (Rutter et al., 1989; Bini et al., 2014, 2017; Zanchetta et al., 2014). Two generations of wedges were identified and interpreted as products of deep seasonal frost action in frozen ground, which produced open cracks that filled rapidly with partially non-local aeolian sediments (Fig. 2). This hypothesis is supported by grain-size (fine sand, moderately sorted) and quartz grain microtexture characteristics of the infilling sediments (Ribolini et al., 2014). Moreover, fragments of Andean volcanic glass shards in the wedge-fill suggest transport via a westerly component of wind direction. The radiocarbon dating of a carbonate crust stratigraphically below the first wedge generation yielded an age of 25,780±160 yr BP. Moreover, the first generation of wedge originated in aeolian sands Optically Stimulated Luminescence (OSL) dated to 14,670±750 yr BP (Ribolini et al., 2014). This was interpreted to indicate that ground wedge formation occurred during a LG cold event, likely correlated to the Antarctic Cold Reversal (ACR) period (12-15 ka BP). The age of the second wedges generation is still undated.

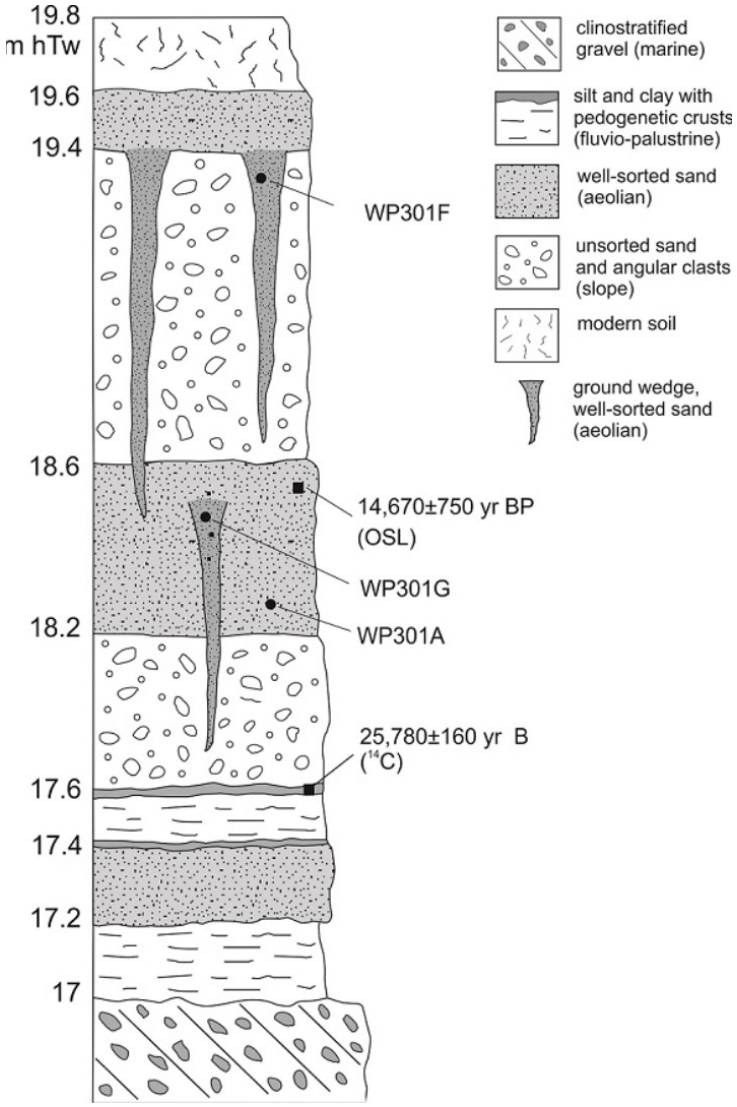

Fig. 2.

Fig. 2. Stratigraphy of the studied section (after Ribolini et al., 2014). Sample position (WP) is also reported. Altitude is reported above meters high Tide water level (m hTw).

3. Methods

The stratigraphy of the studied section is reported in figure 2, with the samples position and the obtained ages by Ribolini et al. (2014). The samples, collected during a field campaign in the 2011, were dried at room temperature and, then, observed and described under a stereomicroscope. A representative fraction of the bulk samples was washed in deionised water to remove the presence of the clay fraction, dried and embedded in epoxy resin, coated with graphite and checked for glass shards using a Scanning Electron Microscopy (SEM) at the Earth Sciences Department of the University of Pisa. Energy-dispersive spectrometry (EDS) of volcanic glass shards was performed using an EDAX-DX micro-analyzer mounted on a Philips SEM 515 (operating conditions: 20 kV acceleration voltage, 100 s live time counting, 200-500 nm beam diameter, 2100-2400 shots s-1, ZAF correction). The ZAF correction procedure does not include natural or synthetic standards for reference, and requires analysis normalization at a given value (chosen at 100%). Detailed discussion on the SEM-EDS performance, inter-calibration trials and standards can be found in Marianelli and Sbrana (1998), Cioni et al. (1998), Caron et al. (2010, 2012), Vogel et al. (2010), Zanchetta et al. (2012).

According to the intercalibration, analytical precision is 0.5% for abundances higher than 15 wt%, 1% for abundances around 5 wt%, 5% for abundances of 1 wt%, and less than 20% for abundances close to the detection limit (around 0.5 wt%). During this work, we used two standards (Albite and CFA47) whose chemistry was accurately controlled and described by Cioni et al. (1998) and Marianelli and Sbrana (1998). Appendix reports the certified values of the standards and the values obtained.

To avoid alkali loss, especially Na, a window spot usually ca. 10 μm wide was used. Due to the different shapes and sizes of glass shards, sometimes a smaller beam size had to be used. The use of smaller beam sizes obligate to reduce the size of the defocused beam and this could influence analytical data due to the complex combination of element mobility and sample damage (Hunt and Hill, 2001).

The major chemical components (SiO2, Al2O3, Na2O, MgO, P2O5, K2O, CaO, TiO2, MnO, Fe2O3T) were determined by X-Ray Fluorescence (XRF) of the bulk samples on fused glass discs utilizing an ARL 9400 XP+ sequential X-ray spectrometer under the instrumental conditions reported in Lezzerini et al. (2013). Within the range of the measured concentrations, the analytical uncertainties are <3% for all the components except for Na2O, P2O5, CaO, TiO2 and MnO which may occasionally attain <10% for very low concentrations (Lezzerini et al., 2013, 2014).

The amount of the volatile components was determined as loss on ignition (LOI in 105-950 °C temperature range). The CO2 content was measured by using the calcimetry method (Leone et al., 1988) on 300 mg of finely powdered samples previously dried at 105±5 °C.

Qualitative mineralogical compositions of the analysed samples were performed by X-Ray Powder-Diffraction analysis (XRPD). X-ray powder diffraction spectra were collected by an automatic diffractometer with Bragg-Brentano geometry, Bruker model D2 PHASER 2nd Generation equipped with a Lynxeye 1D detector and Ni-filtered Cu Kα radiation (λ=1.5406 Å). Data were scanned within the angular range 4-65°(2θ), with a step size of 0.02°(2θ) and a counting time of 0.3 s/step. The Brucker AXS DIFFRAC.EVA software was used for identifying the mineral phases.

4. Results

4.1. Bulk chemical analysis

Three samples were selected for the analyses (Fig. 2): two correspond to distinct sand wedges (sample WP301G, first wedge generation, sample WP301F, second wedge generation) and one comes from a level (sample WP301A) interpreted such as loess by Ribolini et al. (2014). Table 1 shows the chemical result of the major elements. The analyzed samples show some differences on major elements chemistry indicating that the origin of the sediment was little different or they experiences different selection during transport and/or weathering (Fig. 3). XRD patterns are very similar (Fig. 4). They show that quartz, feldspars and phyllosilicates are the main component (Fig. 4).

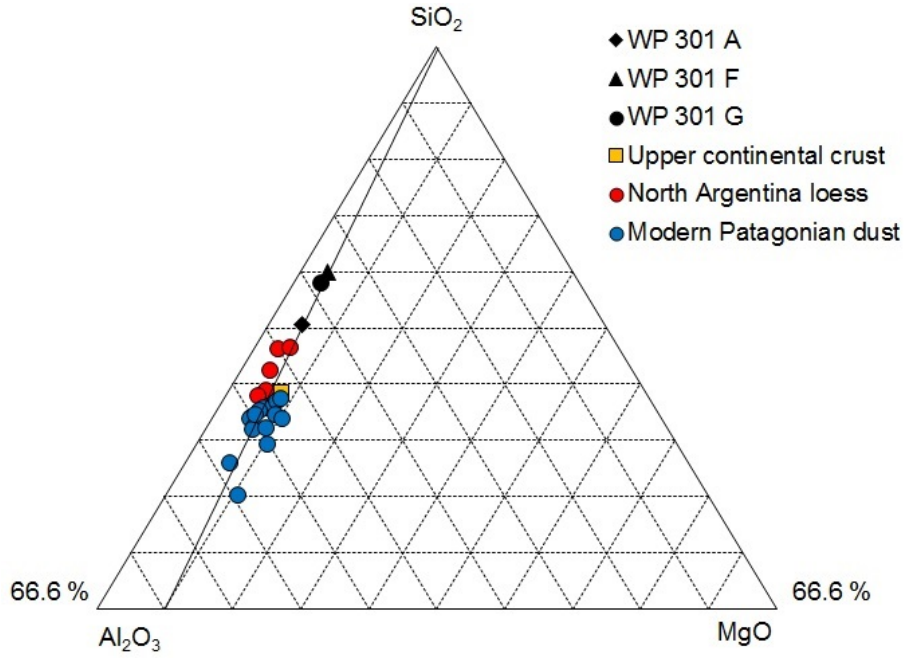

Fig. 3.

Fig. 3. SiO2-Al2O3-MgO diagram of the studied samples. Chemical composition of the upper crust is also shown (Wedepohl, 1995).

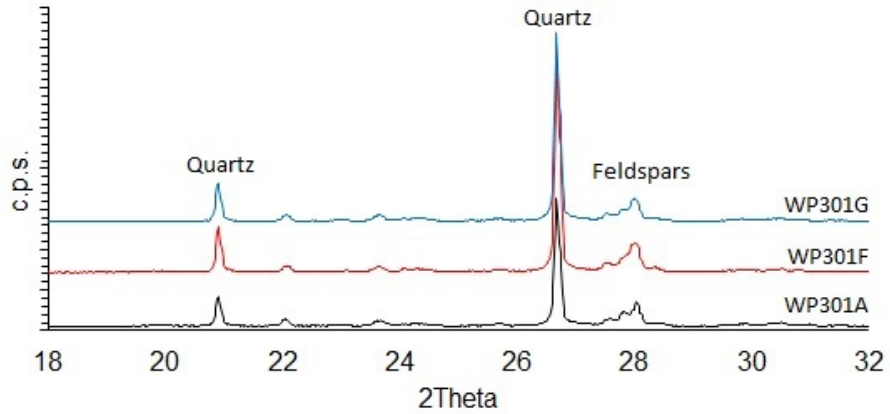

Fig. 4.

Fig. 4. XRD of the studies samples. Most intense XRD reflection of main phases are indicated.

TABLE 1. CHEMICAL DATA OF THE MAJOR ELEMENTS OF THE STUDIED SAMPLES.

Sample	Na_2O	MgO	Al_2O3	SiO_2	P_2O_5	K_2O	CaO	TiO_2	MnO	Fe_2O_3 T	L.O.I.
WP 301 A	2.84	1.39	12.65	71.15	0.09	2.27	2.25	0.72	0.07	4.21	2.36
WP 301 F	2.53	1.15	10.55	76.11	0.09	2.09	1.65	0.50	0.06	3.25	2.02
WP 301 G	2.58	1.23	11.02	75.03	0.10	2.06	2.10	0.68	0.07	3.73	1.40

L.O.I.: loss on ignition at 950 °C; **Fe_2O_3 T:** total iron expressed as Fe_2O_3.

Table 1

4.2. Glass shards characteristics

Volcanic glass shard were found in the infilling of both wedge generations. They exhibit a morphology from micropumices (oval and stretched vesicles) to bubble-wall (Fig. 5a, b, c). The degree of vesicularity varies from

low to relatively high (Fig. 5c, d), and vesicles may be filled by fine grain-size material (Fig. 5a, b). Abundant stretched vesicles give to some glass shard grain a fibrous texture (Fig. 5b). Blocky and non-vesicular plate glass shards with smooth surface and concoidal fracture planes were also found (Fig. 5e, h). Bubble coalescence generates big cavities that together with normal size vesicles determine an irregular general outlines of the grain (Fig. 5f, g). In lesser amounts, more regular prismatic forms were observed (Fig. 5e, h). Over imprinted on the general shape of the grains edge, local irregularities at a higher scale were observed (Fig. 5a, e, g). Some glass shard textures indicate shattering processes. i.e., thermal contraction fractures (Fig. 5h).

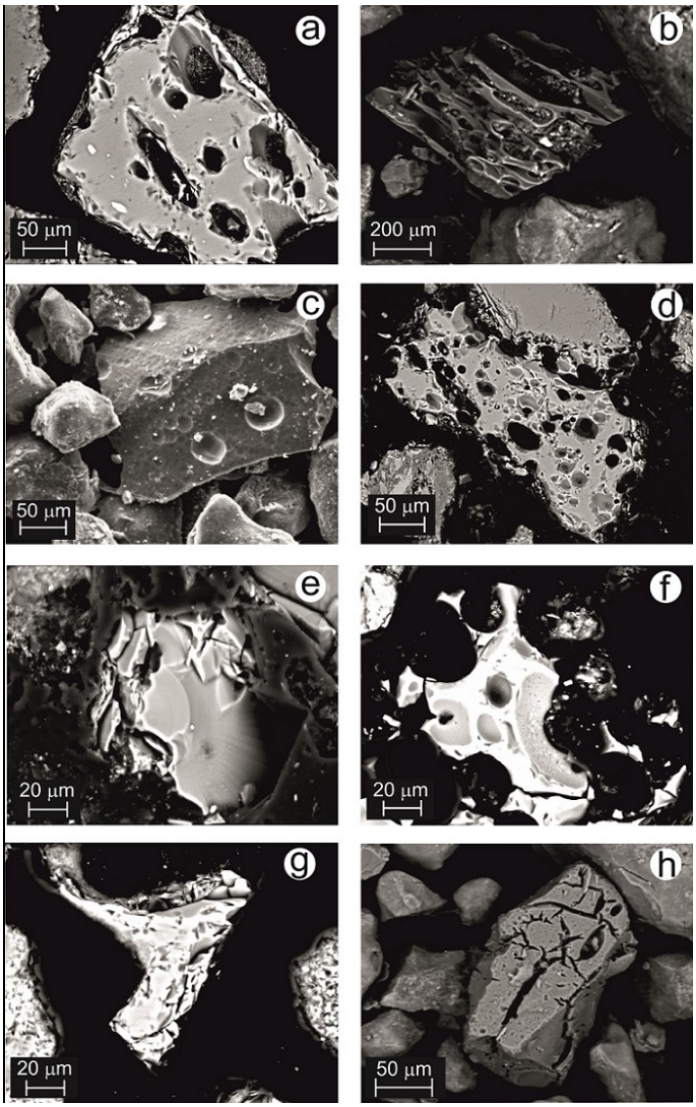

Fig. 5.

Fig. 5. SEM images illustrating the morphology of glass shard found in the ground wedge infillings. a-b. pumiceous morphology with oval (a) (WP301G) and stretched vesicles (b) (WP301G); c-d. bubble-wall morphology with a degree of vesicularly from low (c) (WP301F) to high (d) (WP301G); e. blocky and non-vesicular plate morphology with concoidal fracture planes (WP301F); f. irregular grains outline morphology due to bubble coalescence (301F); g. local outline irregularities over imprinted on the general shape of the grain (WP301F); h. morphology characterized by the effect of shattering processes due to thermal contraction (i.e., irregular thermal fractures) (WP301F).

4.3. Glass shard chemistry

Chemical analysis were undertaken on 22 and 10 volcanic glass shards of the first and second generation of wedges, respectively (Table 2). Because the analyses were not obtained from an enriched fraction this may

qualitatively mean that the sample of the first generation is probably richer in shards than the sample of the second generation. In the Total Alkali Silica diagram (TAS, Le Bas et al., 1986), three main compositional groups are visible, which are present in both wedge generations. The first two groups range from Basaltic andesite to Trachyandesite, with a gap in Silica content, and the last group is formed by samples of glass shards having more evolved trachydacite composition (Fig. 6). A minor group of shards shows typical rhyolitic composition. K2O/Na2O ratio is usually <1, with the exception of two shards with higher silica composition (77.5 and 78%), which show the K2O/Na2O ratio >1 (Table 2).

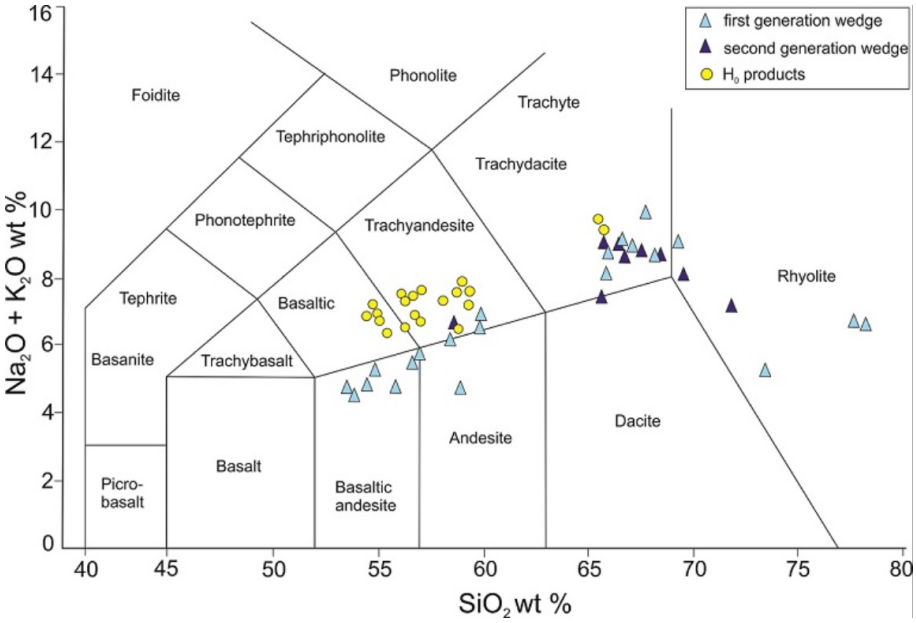

Fig. 6.

Fig. 6. Total Alkali Silica diagram (Le Bas et al., 1986) for the studies glass shards. H0 after Weller et al., 2014.

TABLE 2. CHEMICAL DATA FOR GLASS SHARDS.

Sample	1	2	3	4	5	6	7	8	9	10	11	12	13	14	15	16	17	18	19	20	21	22
WP301F																						
SiO_2	56.84	59.67	59.81	53.76	65.86	69.17	78.1	73.31	55.76	66.44	56.53	68.02	54.72	54.36	77.54	53.42	67.00	58.81	56.49	58.32	67.63	65.79
TiO_2	1.60	1.81	1.51	2.30	1.01	0.57	0.08	0.38	1.59	0.91	1.60	0.59	2.16	1.80	0.22	2.01	0.87	1.22	1.59	1.33	0.71	1.02
Al_2O_3	17.54	15.93	17.12	15.04	16.71	16.10	12.99	14.53	16.96	16.38	17.26	16.70	16.31	16.26	12.90	16.00	16.41	16.20	18.06	17.17	16.30	16.46
FeO_{tot}	7.92	8.00	6.86	10.75	3.65	2.67	1.32	3.47	8.36	3.98	8.26	2.99	9.49	9.92	1.12	10.07	3.41	7.57	7.80	7.65	3.17	4.27
MnO	0.20	0.09	0.25	0.36	0.05	0.00	0.00	0.00	0.17	0.18	0.19	0.00	0.23	0.16	0.00	0.18	0.09	0.13	0.14	0.00	0.05	0.10
MgO	3.34	2.54	2.41	4.56	1.38	0.82	0.21	0.65	4.53	0.88	3.58	1.00	3.76	4.59	0.23	4.77	1.06	4.15	3.50	3.13	0.75	1.18
CaO	6.61	5.09	4.83	8.15	2.46	1.40	0.48	2.20	7.45	1.90	6.82	1.91	7.41	7.70	1.10	8.49	2.10	6.91	6.58	5.98	1.36	2.81
Na_2O	4.38	4.52	4.60	3.09	5.72	6.03	2.65	3.39	3.50	5.82	4.07	5.77	4.02	3.58	3.18	3.36	6.02	3.58	4.12	4.55	6.63	5.28
K_2O	1.44	2.04	2.39	1.48	3.02	3.06	4.00	1.95	1.32	3.38	1.49	2.93	1.28	1.30	3.62	1.47	2.97	1.19	1.40	1.69	3.29	2.93
P_2O_5	0.00	0.25	0.06	0.4	0.00	0.00	0.00	0.00	0.30	0.00	0.16	0.00	0.52	0.30	0.00	0.14	0.00	0.24	0.24	0.11	0.00	0.00
Cl	0.13	0.08	0.16	0.11	0.14	0.18	0.17	0.12	0.06	0.13	0.04	0.09	0.10	0.03	0.09	0.09	0.07	0.00	0.08	0.07	0.11	0.16
Total	100	100	100	100	100	100	100	100	100	100	100	100	100	100	100	100	100	100	100	100	100	100
Na_2O+K_2O	5.82	6.56	6.99	4.57	4.57	9.09	6.66	5.34	4.82	9.20	5.56	8.70	5.30	4.88	6.80	4.83	9.00	4.77	5.52	6.24	9.92	8.21
K_2O/Na_2O	0.33	0.45	0.52	0.48	0.48	0.51	1.51	0.58	0.38	0.58	0.37	0.51	0.32	0.36	1.14	0.44	0.50	0.33	0.34	0.37	0.50	0.55
WP301G																						
SiO_2	56.97	58.58	71.79	66.67	69.53	68.37	65.57	65.68	67.46	66.44	-	-	-	-	-	-	-	-	-	-	-	-
TiO_2	2.11	2.98	0.53	0.95	0.70	0.82	1.20	1.02	0.75	0.89	-	-	-	-	-	-	-	-	-	-	-	-
Al_2O_3	15.75	13.03	14.72	16.85	16.31	16.39	16.53	16.35	16.47	16.55	-	-	-	-	-	-	-	-	-	-	-	-
FeO_{tot}	9.95	10.53	2.91	3.85	2.84	3.04	4.66	4.16	3.65	3.50	-	-	-	-	-	-	-	-	-	-	-	-
MnO	0.07	0.27	0.00	0.19	0.15	0.25	0.30	0.12	0.18	0.11	-	-	-	-	-	-	-	-	-	-	-	-
MgO	2.61	2.77	0.78	1.25	0.76	0.77	1.31	1.15	0.92	1.09	-	-	-	-	-	-	-	-	-	-	-	-
CaO	6.23	4.62	1.87	1.43	1.49	1.54	2.67	2.38	1.64	2.23	-	-	-	-	-	-	-	-	-	-	-	-
Na_2O	3.63	3.80	4.43	7.49	5.07	5.46	4.67	6.51	6.07	6.14	-	-	-	-	-	-	-	-	-	-	-	-
K_2O	2.19	2.94	2.80	1.20	3.06	3.26	2.84	2.55	2.74	2.89	-	-	-	-	-	-	-	-	-	-	-	-
P_2O_5	0.32	0.30	0.00	0.00	0.00	0.00	0.12	0.00	0.00	0.00	-	-	-	-	-	-	-	-	-	-	-	-
Cl	0.17	0.18	0.17	0,12	0.09	0.10	0.13	0.12	0.12	0.16	-	-	-	-	-	-	-	-	-	-	-	-
Total	100	100	100	100	100	100	100	100	100	100	-	-	-	-	-	-	-	-	-	-	-	-
Na_2O+K_2O	5.82	6.74	7.23	8.69	8.13	8.73	7.51	9.06	8.81	9.03	-	-	-	-	-	-	-	-	-	-	-	-
K_2O/Na_2O	0.60	0.77	0.63	0.16	0.60	0.60	0.61	0.39	0.45	0.47	-	-	-	-	-	-	-	-	-	-	-	-

Table 2

5. Discussion

There are slight differences in the major elements composition among the three samples analyzed (Table 1, Fig. 3), suggesting that there were some changes in average composition of the source and/or different sorting processes during the deposition of the aeolian sediment infilling the wedges. Interestingly, the samples show a significant SiO2-enriched composition compared to the most of the loess deposits of the North Argentina (Gallet et al., 1998) and the present day dust originated in different places along the Patagonia (Gaiero et al., 2007) (Fig. 3). This can be explained with a particular prominent local source effect linked to the presence of the rocks of the Chon Aike formation along the Deseado Massif, mostly showing rhyolitic composition and representing one of the largest silicic igneous province of the world (Pankhurst et al., 1998). Pankhurst et al. (1998) noted that many of the rhyolites have been chemically altered by post-emplacement processes showing silica well above the normal maximum of fresh glass of ca. 78 wt%. In addition, below the Chon Aike formation, at places, quartz-rich upper Proterozoic-lower Paleozoic metamorphic and igneous rocks outcrop (Guido et al., 2004).

The presence and relative abundance of quartz mineral in the wedge infilling is also supported by XRD analyses (Fig. 4). These results converge in indicating that the main deflation area for these deposits follow the E-W oriented structural axis of the Deseado massif. However, a more complex Andean source cannot be excluded, like supplied by rivers, which transported high quantity of loose sediment toward the coastal areas during glacial periods (Zarate and Blasi, 1993).

Instead, volcanic component originated from explosive eruption from Andean belt seems to give a very minor "imprinting" to the chemical composition of the sand wedges, both for the low amount of volcanic fragments and for their chemistry (Fig. 6).

The quenching morphology of the glass shards found in the infilling of both wedge generation are indicative of explosive eruptions, with high fragmentation and dispersion. Moreover, shard textures generated by shattering processes may be related to magma having made contact with glacier ice above, and causing fractures due to thermal contraction.

The presence of concoidal fracture planes shown by some fragments points to an aeolian reworking of the volcanic material, that followed an initial deposition and induced the formation of crashing structures. The reworking processes are also confirmed by the indented edges of some shards.

Due to the geographic location of Puerto Deseado, and the main dispersion of explosive eruption (e.g., Scasso et al., 1994; Naranjo and Stern, 1998; Fontijn et al., 2014) the possible eruptive centers can be reasonably limited to the volcanic apparatus belonging to the southern part of the South Volcanic Zone (SVZ) or the northern part of the Austral Volcanic Zone (AVZ) (Corbella and Lara, 2008). Most of the glass shards shows affinity with the products of the Hudson volcano (Naranjo and Stern, 1998), the southernmost volcano of the SVZ (Fig. 1). The Harker diagrams TiO2, CaO, and MgO versus SiO2 sustain the hypothesis that the Hudson is the eruptive center responsible of the glass shard found in the wedges (Fig. 7). Indeed, the found values fall in the specific fields of the Hudson, with characteristic higher values of TiO2 and lower values of CaO and MgO in respect to other volcanoes of the region (e.g., Naranjo and Stern, 1998; D'Orazio et al., 2003; Stern, 2008; Weller et al., 2014). Moreover, Hudson is characterized by higher trends of increasing in K2O compared to the nearby volcanoes (Naranjo and Stern, 1998). The eruption of Hudson volcano, called H0 and dated at 17,300-17,400 cal yr BP (Weller et al., 2014) is the most important documented post-glacial eruption among all the southern Andes (Weller et al., 2014). It fits relatively well with the available chronological data on wedges structures. The first wedge generation must be older than the age of the sandy layer affected by cryogenic structures (14,670±750 yr BP) and the eruption must be younger of the radiocarbon age of the carbonate crust below the first generation of wedges (25,780±160 yr BP) (Ribolini et al., 2014).

The chemical characteristics of H0 show a bimodal compositional distribution in the TAS diagram (Fig. 6), with a part with a basaltic-trachiandesite and glass between 55 and 59 wt% SiO2, and a part with more evolved members up to trachidacites and glass with 66 wt% SiO2 (Weller et al., 2014). A bimodal distribution is observable also in the recent Hudson eruption (H3) occurred in the 1991, but with different proportion among compositions. In the eruptions named H1 and H2 (Holocene), are not observed bimodal distributions (Naranjo and Stern, 1998). In the TAS diagram, the composition of the shards in both wedge generation fairly matches the H0 compositions (Fig. 6), and this supports a possible correlation of the most of the shards analyzed. However, it is worth noting that the less evolved composition appears to have a relatively lower Alkali content compared to the data reported by Weller et al. (2014). Using EDS data is not possible to detect high degree of alteration and it is not surprising that less evolved product can show alkali loss owing to superficial weathering. We have to note, however, that micro-analytical data in recent works suggest a more larger field of composition for the Hudson volcano explosive product (Carel et al., 2011; Stern et al., 2015, 2016), than those reported in Narajo and Stern (1998) and Weller et al. (2014), which can be also supported by our data.

Overall, major elements support the correlation of most of the shards with the Hudson volcanoes and the presence of bimodal composition and chronological constrain strongly support the correlation with H0 eruption, even if part of the glass shards may have experienced some degree of weathering.

Considering the geographic location of the Hudson in respect to the Puerto Deseado area, and being the reported dispersion product of H0 toward NE (Weller et al., 2014), a WNW component in the western wind direction could be hypothesized. This wind component has reworked glass shards and mixed with a dust fraction with strong imprinting generated by the rock deflated over the Deseado Massif structural high. The tephra fall from the August 12-15, 1991 explosive eruption of Hudson volcano involved the Deseado Massif up to the coast (Scasso and Carey, 2005), in agreement with the observation that WNW winds may reach this area.

As already mentioned, in the TAS diagram there is a minor presence of glass shards with a high content of silica (rhyolitic composition) in both wedge generations (Fig. 6). This chemical character may correspond to different volcanoes both in the SVZ and AVZ (Kilian et al., 2003; Watt et al., 2013; Stern, 2008; Wastegård et al., 2013). The very scattered nature in the chemical composition suggests that these shards may represent different sources/eruptions. However, the number of chemical analyses are not suitable for more precise correlations. However, these volcanic shards could suggest long and differential transport also from southern areas.

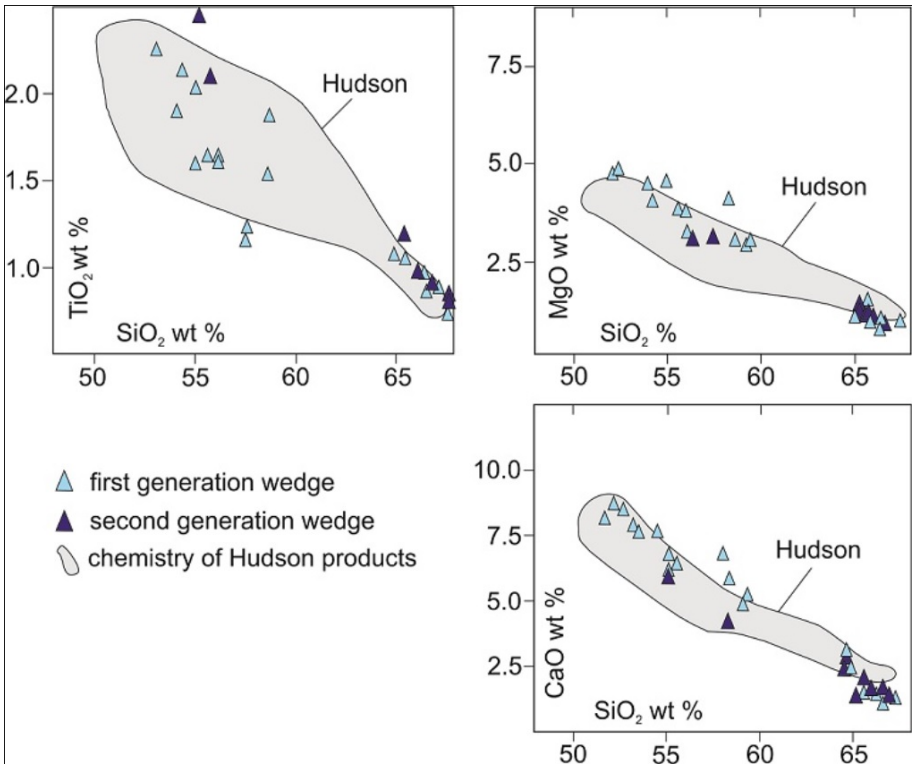

Fig. 7.

Fig. 7. Some Harker diagrams for the glass shards studied. The chemical composition of the Hudson volcano is also shown (after D'Orazio et al., 2003).

6. Conclusion

The studied wedge structures reflect deep, seasonal frost action, with open cracks in the surface of a frozen ground that rapidly filled with sediments not exclusively of local origin (i.e., aeolian). Bulk chemical analyses indicate a very uncommon composition compared to loess from Northern sector of Argentina, and compared to modern Patagonian dust source. This can implies a strong selection of infilling material favoring the Silica-rich (i.e., quartz) material, which can be explained such as a provenance mostly controlled by the rock outcropping over the Deseado Massif.

Chemical analyses of glass shards indicate that most of the glass shards are originated by the Hudson volcano. Chemical and chronological constraints strongly support the correlation of most of the shards with H0 eruption (17,300-17,400 cal yr BP). This indicates that aeolian process reworked the H0 volcanic products and filled the frost cracks opened into the ground during the LG, and these shards represented a long available material for transportation. While the H0 further constraints the first generation of wedges to the Antarctic Cold Reversal (ACR) period, the age of the second generation remains uncertain.

This study underlines how geochemical analyses of the sediments infilling of ground wedge can be associated to the classic studies, i.e., geomorphology, stratigraphy, grain-size, quartz-grain texture, to retrieve relevant information about the geomorphological processes and their chronology. These results are particularly promising due to the relative abundance of wedge structures along the Patagonia, whose infilling sediments have potentially recorded Late Pleistocene volcanic events and different sources of aeolian deflation and, hence, providing chronological constraints and indications about wind direction and intensity.

Acknowledgements

We thank J. Cause and the no-profit organization CADACE for the logistical support in the field campaign. This work was funded by the University of Pisa (Progetto Ateneo 2007, Leader G. Zanchetta; Progetto Ateneo PRA 2014 Leader G. Zanchetta) and MIUR (PRIN2008, Leader G. Zanchetta). We thank C.R. Stern for the comment and review of the manuscript, which improved the quality of the manuscript.

References

Bini, M.; Isola, I.; Pappalardo, M.; Ribolini, A.; Favalli, M.; Ragaini, L.; Zanchetta, G. 2014. Abrasive notches along the Atlantic Patagonian coast and their potential use as sea level markers: the case of Puerto Deseado (Santa Cruz, Argentina). Earth Surface Processes and Landforms 39: 1550-1558.

Bini, M.; Zanchetta, G.; Ribolini, A.; Salvatore, M.C.; Pappalardo, M.; Baroni, C.; Isola, I.; Isla, I.F.; Fuck, E.; Boretto, G.; Morigi, C.; Ragaini, L.; Marzaioli, F.; Passariello, I. 2017. Last interglacial sea-level highstand deduced from notches and inner margins of marine terraces at Puerto Deseado, Santa Cruz Province, Argentina. Geografia Fisica e Dinamica Quaternaria 40: 27-39.

Bockheim, J.; Coronato, A.; Rabassa, J.; Ercolano, B.; Ponce, J. 2009. Relict sand wedges in southern Patagonia and their stratigraphic and paleo-environmental significance. Quaternary Science Reviews 28: 1188-1199.

Carel, M.; Siani, G.; Delpech, G. 2011. Tephrostratigraphy of a deep-sea sediment sequence off the south Chilean margin: New insight into the Hudson volcanic activity since the last glacial period. Journal of Volcanology and Geothermal Research 208: 99-111.

Caron, B.; Sulpizio, R.; Zanchetta, G.; Santacroce, R. 2010.The Late Holocene to Pleistocene tephrostratigraphic record of Lake Ohrid (Albania). Comptes Rendus Geosciences 342: 453-466.

Caron, B.; Siani, G.; Sulpizio, R.; Zanchetta, G.; Paterne, M.; Santacroce, R.; Tema, E.; Zanella, E. 2012. Late Pleistocene to Holocene tephrostratigraphic record from the Northern Ionian Sea. Marine Geology 311-314: 41-51.

Cioni, R.; Marianelli, P.; Santacroce, R. 1997. Thermal and compositional evolution of the shallow magma chambers of Vesuvius: evidence from pyroxene phenocrysts and melt inclusions. Journal of Geophysical Research 103: 18277-18294.

Corbella, H.; Lara, L.E. 2008. Late Cenozoic Quaternary Volcanism in Patagonia and Tierra del Fuego. In "The Late Cenozoic of Patagonia and Tierra del Fuego" (Rabassa J.; editor). Developments in Quaternary Science 11: 95-119.

Corte, A.; Beltramone, C. 1984. Edad de las estructuras geocriogénicas de Puerto Madryn, Chubut, Argentina. Acta Geocriogénica 2: 67-72.

Coronato, A.; Bujalesky, G.; Pérez Alberti, A.; Rabassa, J. 2004. Evidencias criogénicas fósiles en depósitos marinos interglaciarios de Tierra del Fuego, Argentina. In Reunión Argentina de Sedimentologia, No. 10: 48-49. San Luis.

Czajka, W. 1955. Rezente und pleistozäne Verbreitung und Typen des periglazialen Denudationszyklus in Argentinien. Acta Geographica 14: 121-140.

D'Orazio, M.; Innocenti, F.; Manetti, P.; Tamponi, M.; Tonarini, S.; González-Ferrán, O.; Lahsen, A.; Omarini, R. 2003. The Quaternary cal-alkaline volcanism of the Patagonian Andes close to the Chile triple junction: geochemistry and petrogenesis of volcanic rocks from Cay and Maca volcanoes (~45° S, Chile). Journal of South American Earth Sciences 16: 219-242.

Fontijn, K.; Lachowycz, S.M.; Rawson, H.; Pyle, D.M.; Mather, T.A.; Naranjo, J.A.; Moreno-Roa, H. 2014. Late Quaternary tephrostratigraphy of southern Chile and Argentina. Quaternary Science Reviews 89: 70-84.

French, H. 2011. Frozen sediments and previously-frozen sediments. Geological Society, Special Publications 354: 153-166. London.

French, H.; Demitroff, M.; Newell, W.L. 2009. Past Permafrost on the Mid-Atlantic Coastal Plain, Eastern United States. Permafrost and Periglacial Processes 20: 285-294.

Gaiero, D.M.; Brunet, F.; Probst, J.-L.; Depetris, P.J. 2007. A uniform isotopic and chemical signature of dust exported from Patagonia: Rock sources and occurrence in southern environments. Chemical Geology 238: 107-120.

Gallet, S.; Jahn, B.-M.; Van Vliet Lanoë, B.; Dia, A.; Rossello E. 1998. Loess geochemistry and its implications for particle origin and composition of the upper continental crust. Earth Planetary Science Letters 156: 157-172.

Guido, D.; Escayola, M.; Schalamuk, I. 2004. The basement of the Deseado Massif at Bahía Laura, Patagonia, Argentina: A proposal for its evolution. Journal of South American Earth Science 16: 567-577.

Hunt, J.B.; Hill, P.G. 2001. Tephrological implications of beam size-sample-size effects in electron microprobe analysis of glass shards. Journal of Quaternary Science 16: 105-117.

Kilian, R.; Hohner, M.; Biester, H.; Wallrabe-Adams, H.J.; Stern, C.R. 2003. Holocene peat and lake sediment tephra record from the southernmost Chilean Andes (53-55 °S). Revista Geológica de Chile 30 (1): 23-37. doi: 10.5027/andgeoV30n1-a02.

Lachenbruch, A.H. 1962. Mechanics of thermal contraction cracks and ice-wedge polygons in permafrost. Geological Society of America, Special Paper 70: 1-66.

Le Bas, M.J.; Le Maitre, R.W.; Streckheisen, A.; Zanettin, B. 1986. Chemical classification of volcanic rocks based on the total alkali-silica diagram. Journal of Petrology 27: 745-750.

Leone, G.; Leoni, L.; Sartori, F. 1988. Revisione di un metodo gasometrico per la determinazione di calcite e dolomite. Atti Società Toscana Scienze Naturali Memorie, Serie A 95: 7-20.

Lezzerini, M.; Tamponi, M.; Bertoli, M. 2013. Reproducibility, precision and trueness of X-ray fluorescence data for mineralogical and/or petrographic purposes. Atti Società Toscana Scienze Naturali Memorie, Serie A 120: 67-73.

Lezzerini, M.; Tamponi, M.; Bertoli, M. 2014. Calibration of XRF data on silicate rocks using chemicals as in-house standards. Atti Società Toscana Scienze Naturali, Memorie, Serie A 121: 65-70.

Marianelli, P.; Sbrana, A. 1998. Risultati di misure di standard di minerali e di vetri naturali in microanalisi a dispersione di energia. Atti Società Toscana Scienze Nataturali, Memorie Serie A 105: 57-63.

Murton, J.B.; Kolstrup, E. 2003. Ice-wedge casts as indicators of palaeotemperatures: precise proxy or wishful thinking? Progress in Physical Geography 27: 155-170.

Murton, J.B.; Worsley, P.; Gozdzik, J. 2000. Sand veins and wedges in cold aeolian environments. Quaternary Science Reviews 19: 899-922.

Naranjo, J.A.; Stern, C.R. 1998. Holocene explosive activity of Hudson Volcano, southern Andes. Bulletin of Volcanology 59: 291-306.

Pankhurst, R.; Rapela, C. 1995. Production of Jurassic rhyolite by anataxis of the lower crust of Patagonia. Earth and Planetary Science Letters 134: 23-36.

Pankhurst, R.; Leat, P.; Sruoga, P.; Rapela, C.; Márquez, M.; Storey, B.; Riley, T. 1998. The Chon Aike province of Patagonia and related rocks in West Antartica: a silicic large igneous province. Journal of Volcanology and Geothermal Research 81: 113-136.

Pérez-Alberti, A.; Coronato, A.; Valcarcel-Díaz, M.; Rabassa, J. 2008. Wedge structures in the Southernmost Argentina (Río Grande, Tierra del Fuego). Ninth International Conference on Permafrost, Fairbanks, University of Alaska 1381-1385. Alaska.

Ramos, V.A.; Ghiglione, M.C. 2008. Tectonic evolution of the Patagonian Andes. In The late Cenozoic of Patagonia and Tierra del Fuego (Rabassa, J.; editor). Developments in Quaternary Science 11: 57-71.

Ribolini, A.; Bini, M.; Consoloni, I.; Isola, I.; Pappalardo, M.; Zanchetta, G.; Fucks, E.; Panzeri, L.; Martini, M.; Terrasi, F. 2014. Late-Pleistocene wedge structures along the Patagonian coast (Argentina): chronological constraints and palaeo-environmental implications. Geografiska Annaler, Series A, Physical Geography 96: 161-176.

Rutter, N.; Schnack, E.J.; del Rio, J.; Fasano, J.L.; Isla, I.F.; Radke. U. 1989. Correlation and dating of Quaternary littoral zones along the Patagonian coast, Argentina. Quaternary Science Reviews 8: 213-234.

Schellmann, G. 1998. Jungkänozonische Landschaftsgeschichte patagoniens (Argentinien). Andine Vorlandvergletchenrungen, Talentwicklung und marine Terrassen. Essener Geographische Arbeiten 29. Essen.

Scasso, R.A.; Corbella, H.; Tiberi, P. 1994. Sedimentological analysis of the tephra from the 12-15 August l991 eruption of Hudson volcano. Bulletin of Volcanology 56: 121-132.

Scasso, R.; Carey, S. 2005. Morphology and formation of glassy volcanic ash from the Augist 12-15, 1991 eruption of Hudson Volcano, Chile. Latin American Journal of Sedimentology 12: 3-21.

Sruoga, P.; Rubinstein, N.; Hinterwimmer, G. 2004. Porosity and permeability in volcanic rocks: A case study on the Serie Tobífera, South Patagonia, Argentina. Journal of Volcanology and Geothermal Research 132: 31-43.

Stern, C.R. 2008. Holocene tephrochronology record of large explosive eruptions in the southernmost Patagonian Andes. Bulletin of Volcanology 70: 435-454.

Stern, C.R.; de Porras M.E.; Maldonado A. 2015. Tephrochronology of the upper Río Cisnes valley (44°S), southern Chile. Andean Geology 42 (2): 173-189. doi: 10.5027/andgeoV42n2-a02.

Stern, C.R.; Moreno, P.I.; William, I.; Henríquez, W.I.; Villa-Martínez, R.; Sagredo, E.; Aravena, J.C.; de Pol-Holz, R. 2016. Holocene tephrochronology around Cochrane (~47° S), southern Chile. Andean Geology 43 (1): 1-19. doi: 10.5027/andgeoV43n1-a01.

Trombotto, D. 2002. Inventory of fossil cryogenic forms and structures in Patagonia and the mountains of Argentina beyond the Andes. South American Journal of Earth Sciences 98: 171-180.

Trombotto, D.; Ahumada, A.L. 1995. Análisis de estructuras sedimentarias en los 'Rodados Patagónicos' causadas por la presencia del permafrost en el criómero Penfordd, Puerto Madryn, Nordpatagonia. Revista Chilena de Historia Natural 68: 79-91.

Vogel, H.; Zanchetta, G.; Sulpizio, R.; Wagner, B.; Nowaczyk, N. 2010. A tephrostratigraphic record for the last glacial-interglacial cycle from Lake Ohrid, Albania and Macedonia. Journal of Quaternary Science 25: 320-338.

Vogt, T.; del Valle, H.F. 1994. Calcretes and cryogenic structures in the area of Puerto Madryn (Chubut, Patagonia, Argentina). Geografiska Annaler, Series A, Physical Geography 76A: 57-75.

Wastegård, S.; Veres, D.; Kliem, P.; Hahn, A.; Ohlendorf C.; Zolitschka, B.; The PASADO Science Team 2013. Towards a late Quaternary tephrochronological framework for the southernmost part of South America e the Laguna Potrok Aike tephra record. Quaternary Science Reviews 71: 81-90.

Watt, S.F.L.; Pyle, D.M.; Mather, T.A. 2013. Evidence of mid- to late-Holocene explosive rhyolitic eruptions from Chaitén Volcano, Chile. Andean Geology 40 (2): 216-226. doi: 10.5027/andgeoV40n2-a02.

Wedepohl, K.H. 1995. The composition of the continental crust. Geochimica et Cosmochimica Acta 59: 1217-1232.

Weller, D.; Miranda, C.G.; Moreno, P.I.; Villa-Martínez, R.; Stern C.R. 2014. The large late-glacial Ho eruption of the Hudson volcano, southern Chile. Bulletin of Volcanology 76: 1-18.

Williams, P.J.; Smith, M.W. 1989. The Frozen Earth: Fundamentals of Geocryology. Cambridge University Press: 306 p. Cambridge.

Zanchetta, G.; Giraudi, C.; Sulpizio, R.; Magny, M.; Drysdale, R.N.; Sadori, L. 2012. Constraining the onset of the Holocene "Neoglacial" over the central Italy using tephra layers. Quaternary Research 78: 236-247.

Zanchetta, G.; Bini, M.; Isola, I.; Pappalardo, M.; Ribolini, A.; Consoloni, I.; Boretto, G.; Fucks, E.; Ragaini, L.; Terrasi, F. 2014. Middle-to late-Holocene relative sea-level changes at Puerto Deseado (Patagonia, Argentina). The Holocene 24: 307-317.

Zarate, M.; Blasi, A. 1993. Late Pleistocene-Holocene eolian deposits of the southern Buenos Aires Province, Argentina: a preliminary model. Quaternary International 17: 15-20.

Appendix

APPENDIX. COMPARISON BETWEEN STANDARD VALUES CERTIFIED AND MEASURED.

	Certified*	Measured
Albite		
SiO_2	68.15	68.05
Al_2O_3	19.77	20.01
CaO	0.38	0.21
Na_2O	11.46	11.42
K_2O	0.23	0.31
CFA47		
Na_2O	5.40	5.18
MgO	0.42	0.58
Al_2O_3	18.62	18.61
SiO_2	61.94	61.84
Cl	0.49	0.50
K_2O	8.02	8.09
CaO	1.85	1.89
TiO_2	0.42	0.41
MnO	0.18	0.19
FeO	2.66	2.70
Scapolite		
Na_2O	14.77	14.48
MgO	0.01	0.00
Al_2O_3	28.97	28.93
SiO_2	33.28	33.64
S	3.44	3.38
Cl	5.2	5.18
K_2O	0.56	0.58
CaO	13.68	13.68
TiO_2	0.02	0.00
MnO	0	0.00
FeO	0.07	0.15

* see also Cioni *et al.*, 1997.

Appendix